ACS APPLIED MATERIALS & INTERFACES

Letter

www.acsami.org

Construction of Teethlike Homojunction BiOCl (001) Nanosheets by Selective Etching and Its High Photocatalytic Activity

Sunxian Weng,[†] Zhibin Fang,[†] Zhenfeng Wang,[†] Zuyang Zheng,[†] Wenhui Feng,[†] and Ping Liu*[,†]

[†]Research Institute of Photocatalysis, State Key Laboratory of Photocatalysis on Energy and Environment, College of Chemistry, Fuzhou University, Fuzhou 350002, P. R. China

Supporting Information

ABSTRACT: Teethlike homojunctions BiOCl (001) nanosheets with tunable photoresponse were constructed by selective etching with triethanolamine and allowed fast charge separation across the interfaces to facilitate photocatalysis. The unique microstructure exhibits a superior photocatalytic activity that can be ascribed to the combined interaction of the high UV/vis light harvest, high photogenerated charge separation efficiency, and the fast interfacial charge-transfer rate based on the unique homogeneous topotactic structure. We believe that the creation of this new model junction may be a great aid in the design and preparation of efficient semiconductor based photocatalysts and a new understanding of the essential relation between the junction and the photocatalytic activity.

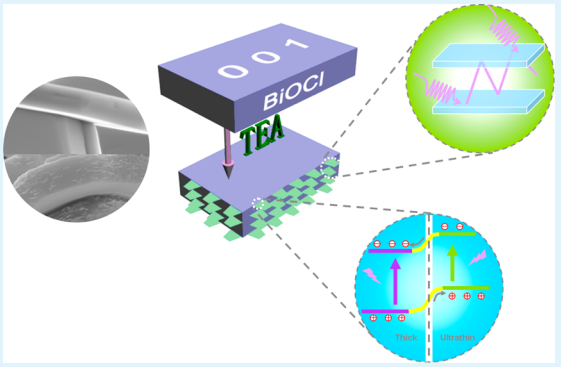

KEYWORDS: *BiOCl (001), homojunctions, etching, triethanolamine, photocatalyst*

Two-dimensional (2D) nanosheets have attracted considerable attention recently because of their unique optical and electronic properties,[1] as well as their promising applications in solar cells, environmental purification, and water splitting.[2,3] Among various 2D nanosheets, the BiOCl nanosheet, a novel layered ternary semiconductor, has been drawn much attention for its remarkable photocatalytic performance, which is comparable to or even better than that of TiO_2 because of its open crystalline structure.[4−10] However, the efficiency of BiOCl nanosheets is still far from satisfaction owing to the rapid recombination of photogenerated excitons and the indigent harvest of sunlight. In practice, the achievement of the photoconversion efficiency generally necessitates the spatial integration of two semiconductors with different properties to form surface heterojunction, so as to optimize the harvest of light, facilitate the accumulation and separation of charge at the interfaces and improve surface catalytic kinetics.[11] Recently, many kinds of heterojunction semiconductors (such as antisotype p-n, isotype n-n, and crystal-phase junctions)[11−18] have been gradually extended to the field of photocatalysis for environmental decontamination and water splitting. However, fabricating efficient junctions for the photocatalytic reaction still remains a challenge since the construction of efficient junctions between two well-matched semiconductors is not only governed by their crystal structure but also by other properties (e.g., electronic structure, band position, and work function).[19]

The pioneering works have found that the thickness of BiOCl nanosheets exposing (001) facets is easily tuned by facile chemical methods based on the stacking of $[Bi_2O_2]^{2+}$ layers between two slabs of Cl^- along with *c* axis and exhibits different properties, including band position and work function.[20] Stimulated by band alignment strategy, the integration of two different thickness BiOCl (001) nonosheets will be a promising approach to enhance the photoconversion efficiency. On the one hand, such a topology-induced staggered band offers an extra chance for the facile engineering of isotype junctions based on BiOCl semiconductors, without depending on adventitious materials. Importantly, the identical crystal structure is able to supply barrier-free tight contact at interfaces which is different from traditional heterojunctions. On the other hand, ultrathin BiOCl (001) nanosheets can diminish the light blocking effect, thus improving the light utilization. It is particularly noteworthy that the creation of this new model junction may be a great aid in the design and preparation of efficient semiconductor based photocatalysts and a new understanding of the essential relation between the junction and the photocatalytic activity.

In this communication, we fabricated a new type of photocatalyst, i.e., teethlike layered BiOCl (001) nanosheets (denoted as T-BiOCl (001)), in which large number of teethlike ultrathin nanosheets are integrated to a thick nanosheets without any traditional heterojunctions. To achieve the unique topotactic structure, the fringe planes of thick nanosheets are etched using triethanolamine (TEA) without damaging (001) plane. The detailed preparation and material characterization are listed in the Supporting Information.

Received: August 5, 2014
Accepted: October 20, 2014
Published: October 20, 2014

   dx.doi.org/10.1021/am5052526 | *ACS Appl. Mater. Interfaces* 2014, 6, 18423−18428

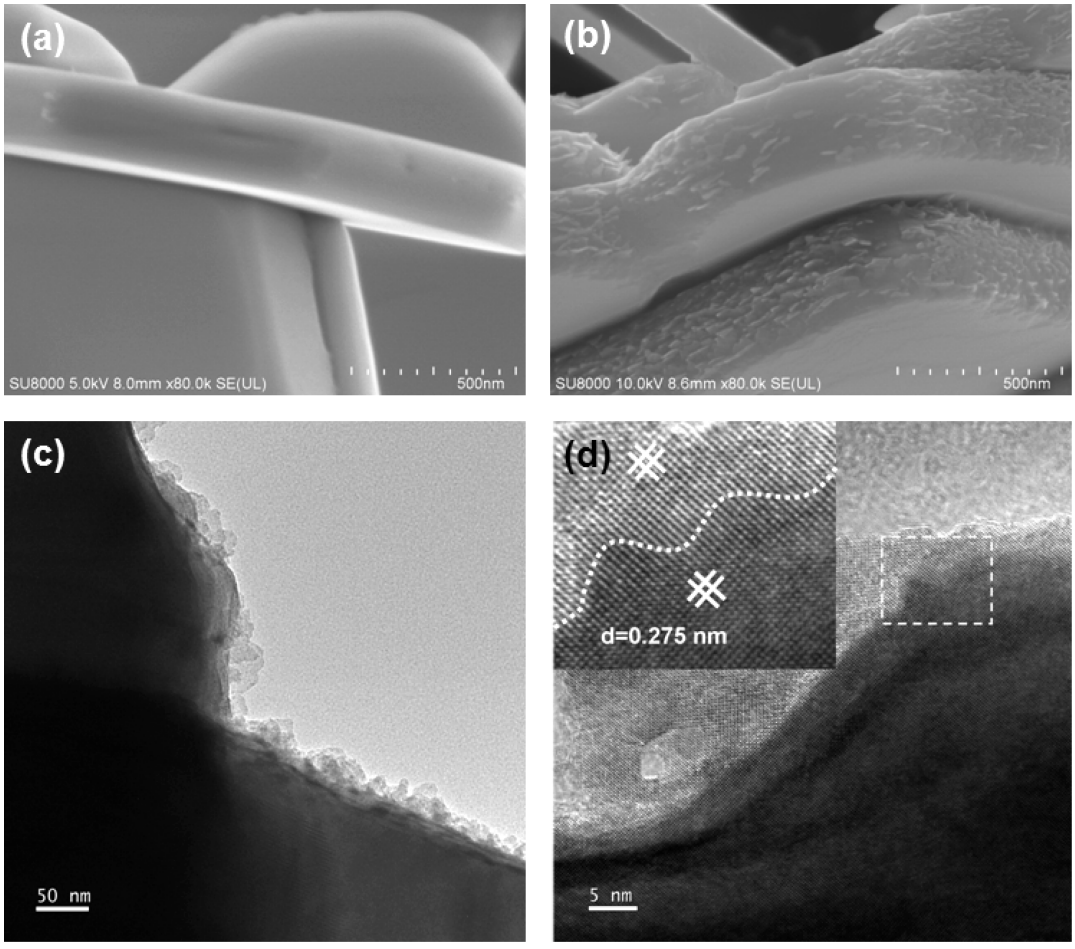

Figure 1. (a) SEM images of BiOCl (001), (b) SEM images, (c) TEM image, and (d) HRTEM images of T-BiOCl (001).

A typical SEM image (Figure 1b) displays that the surface morphological feature of T-BiOCl (001) consists of plentiful thin-scale teethlike nanosheets attached to the fringe planes of large-scale nanosheets, which is quite different from that of pure smooth BiOCl (001) (Figure 1a), indicating that the selective etching with TEA can significantly change the texture of BiOCl (001). And the thickness of ultrathin BiOCl nanosheets is roughly estimated below 10 nm according to SEM image. The detailed morphology of as-fabricated T-BiOCl (001) is also characterized by TEM, as displayed in Figure 1. The high-resolution TEM (HRTEM) images (Figure 1c, d) reveal the crystalline and clear lattice fringes projected along the [001] zone axis both in ultrathin teethlike nanosheets and thick nanosheets. Two sets of lattice fringes with the same interplanar lattice spacing of 0.275 nm correspond to the (1−10) and (110) atomic planes of BiOCl. The angle between the (001) and (110) facets is 90° for the tetragonal structure of BiOCl.[5,9,10,20] It means that the set of diffraction spots can be indexed as the [001] zone axis, which agrees well with the XRD results. In addition, the homojunction is constructed by selective in situ etching on one substrate to obtain two components with different properties, rather than conventional commixture via exogenous process,[12−14] so there should not be disordered interface. The consecutive lattice fringes indicate the tight contact between ultrathin nanosheets and thick nanosheets without any barrier. The virtually identical XRD patterns (see Figure S2 in the Supporting Information), Raman spectroscopy (see Figure S3 in the Supporting Information) and FT-IR spectra (see Figure S4 in the Supporting Information) of BiOCl (001) and T-BiOCl (001) indicate that this etching method does not change the bulk crystal structure of BiOCl (001) and no residual TEA molecules exist on T-BiOCl (001) surface. These findings will scientifically disclose the mechanism for the formation of the unique morphological feature.

It is of great interest to propose the formation mechanism of the T-BiOCl (001), as is illustrated in Figure 2. Experimental and theoretical researches have demonstrated that the surface of BiOCl (001) atomic planes mainly consists of terminal oxygen atoms, and the other fringle planes are surrounded by terminal bismuth atoms and other atoms (see Figure S5 in the Supporting Information). Triethanolamine [N $(CH_2-CH_2-OH)_3$] as a complexing agent to arrest Bi^{3+} has been reported (see Figure S6 in the Supporting Information).[21] Bi (III) combined with TEA is via nitrogen-donor. Thus, the fringe planes of BiOCl (001) exposing terminal bismuth easily combine with TEA and then rapidly dissolve to solution. Meanwhile, the BiOCl (001) planes are perfectly retained because the electrostatic repulsive interaction between TEA ion and terminal oxygen atoms on (001) planes. This unique topotactic structure will possess some particular properties as compared to smooth bulk, suggesting great potential in photocatalytic applications.

The distinguishing optical properties and valence band (VB) of BiOCl (001) before and after treatment are characterized by UV/vis absorption spectra (Figure 3a) and XPS valence spectra

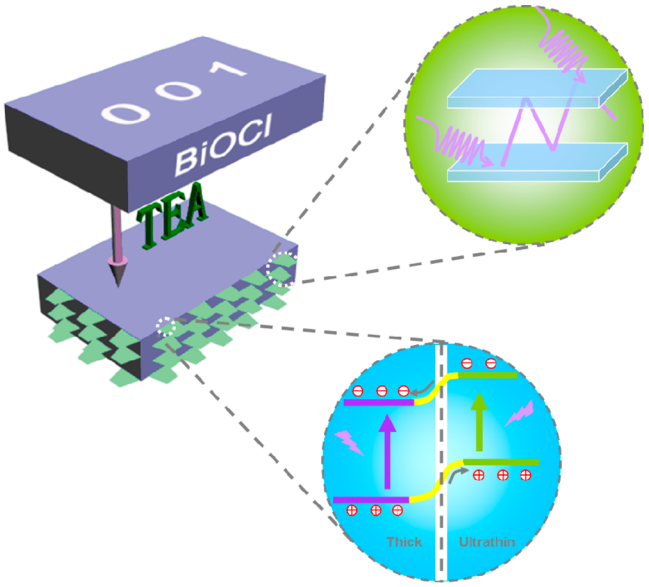

Figure 2. Tentative formation mechanism of the T-BiOCl (001) (left) light paths within the teethlike structure (right up) and the possible charge separation process between thick and ultrathin nanosheets[6] (bottom right).

(Figure 3b), respectively. It can be observed that the band gap of T-BiOCl (001) is similar to BiOCl (001). The BiOCl (001) display a VB with the edge of the maximum energy at about 2.34 eV (Figure 3b). However, for the T-BiOCl (001), the VB maximum energy up-shifts by 0.36 to 1.98 eV compared with that of BiOCl (001), which can be ascribed to the introduction of ultrathin BiOCl nanosheets that possessing higher VB energy than thick ones (Figure 2 bottom right).[20] The staggered band positions[20] of ultrathin BiOCl nanosheets and thick ones which would introduce a new internal electrical field to increase the charge accessible tunnel and lessen the barrier for charge transfer, thus reducing the recombination of the photogenerated excitons. These advantages are confirmed by the following experiments. Moreover, the UV and visible absorption intensity of T-BiOCl (001) is obviously stronger than BiOCl (001). This enhancement in entire wavelength is most likely due to the multi reflection of light in the teethlike morphology[22] and diminishing of the light blocking effect on ultrathin layer (Figure 2 right up), suggesting it a probable higher photocatalytic activity for target reactions by harvesting more light.

Remarkably, the unique topotactic structure which has the identical lattice constants of ultrathin and thick nanosheets, can sustain the formation of homogeneous structure and boost the interfacial charge transfer by the electron tunnelling effect. This photogenerated charges separation efficiency can be confirmed by the photoluminescence (PL) spectra (Figure 3c) and fluorescence decay curves (Figure 3d). Obviously, the T-BiOCl (001) show significantly diminished PL intensity as compared to pure BiOCl, indicating a remarkable decline in charge recombination. The experimental decay profiles of BiOCl (001)

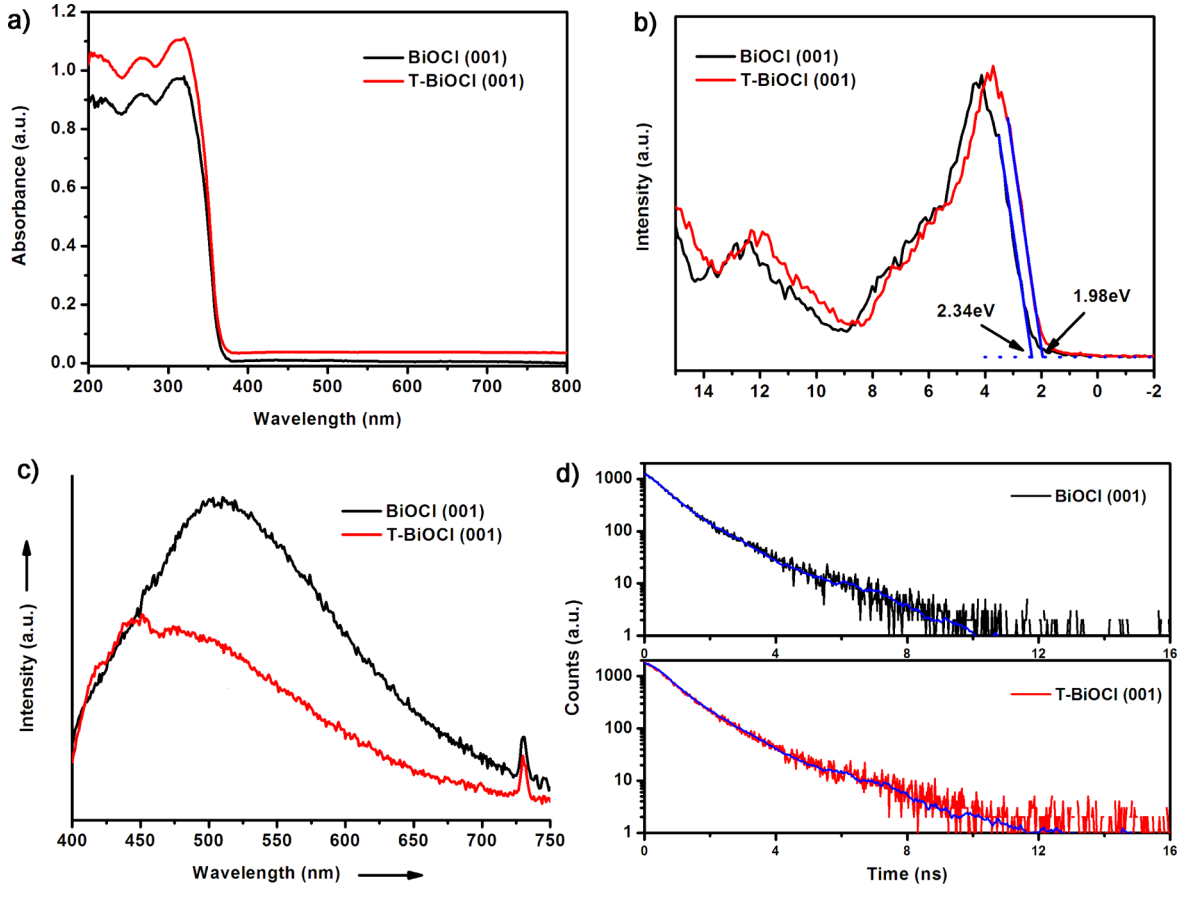

Figure 3. (a) UV−visible DRS, (b) valence-band XPS spectra, (c) photoluminescence spectra, and (d) fluorescence decay curves of BiOCl (001) and T-BiOCl (001).

dx.doi.org/10.1021/am5052526 | ACS Appl. Mater. Interfaces 2014, 6, 18423−18428

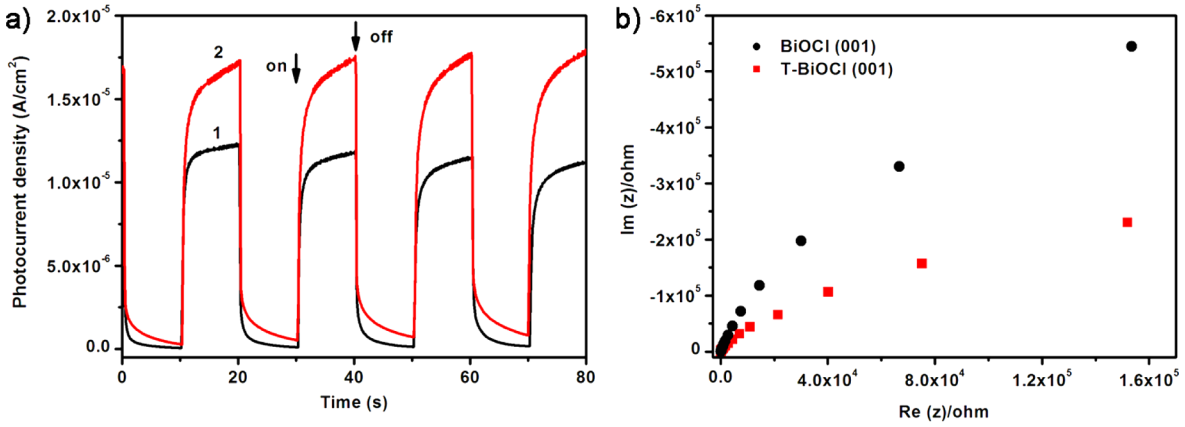

Figure 4. (a) Transient photocurrent responses and (b) Nyquist impedance plots of (1) BiOCl (001) and (2) T-BiOCl (001).

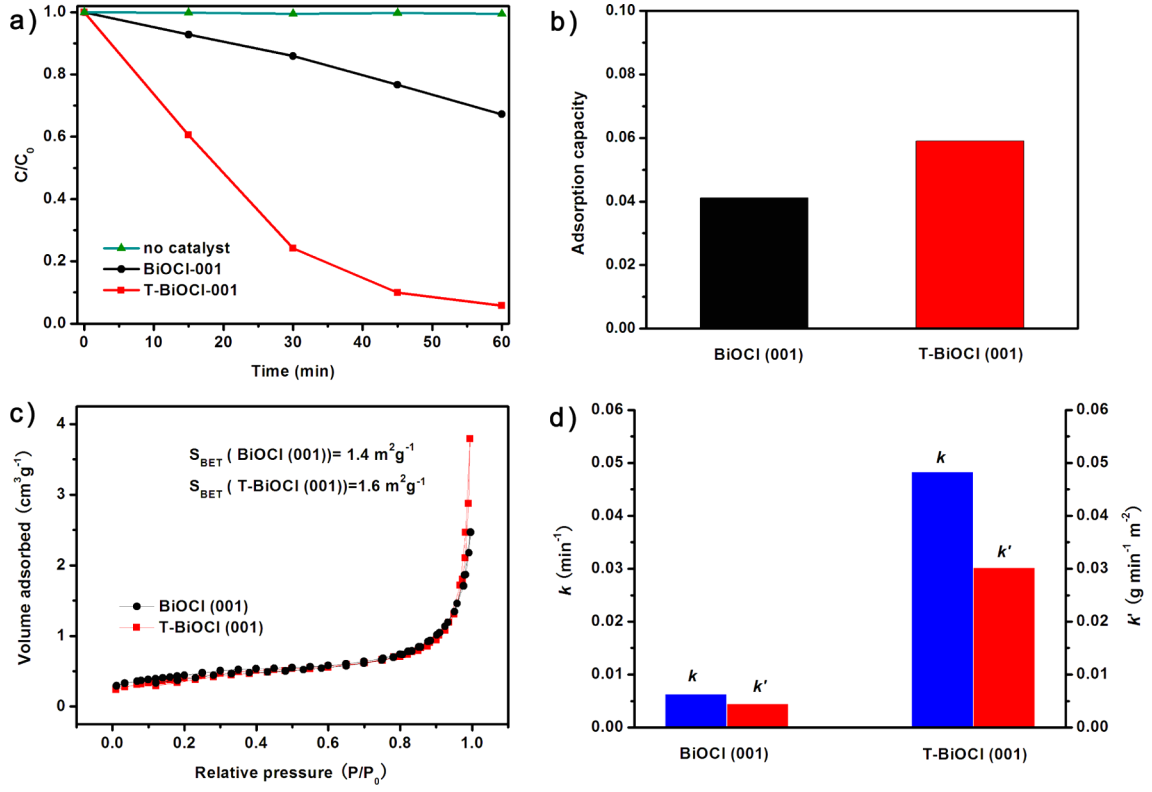

Figure 5. (a) Time profiles of photocatalytic degradation of MO over the samples under UV light irradiation. (b) Time profiles of adsorption of MO over the samples in the dark. (c) Nitrogen adsorption−desorption isotherm of the samples. (d) Comparison on the reaction rate constants for photocatalytic degradation of MO over the samples.

and T-BiOCl (001) are fitted as a multiexponential function (see Table S1 in the Supporting Information). The T-BiOCl (001) show a longer average lifetime ($\langle\tau\rangle$) of 0.22 ns than that of BiOCl (001) (0.19 ns). This occurrence is attributed to the efficient interfacial charge transfer in fringe homogeneous structure of T-BiOCl (001), thus leading to an improvement in the separation efficiency and lifetime of the photogenerated carriers. This photogenerated charge separation efficiency can also be further confirmed by electrochemical measurements.

Electrochemical measurements are conducted in a typical three-electrode cell. A photocurrent when photogenerated charge carriers are transferred between the surface of the electrode and the underlying substrate. Both electrodes are prompt in generating photocurrent with a reproducible response to on/off cycles (Figure 4a), but the T-BiOCl (001) film electrode exhibited a higher photocurrent than the BiOCl (001) film electrode, indicating the more efficient interfacial photoinduced charge separation and transfer by the electron tunnelling effect in T-BiOCl (001). The charge transfer rate in the dark was studied by electrochemical impedance spectroscopy (EIS; Figure 4b) and the expected semicircular Nynquist plots for BiOCl (001) and T-BiOCl (001), with a significantly decreased arc for T-BiOCl (001), are obtained. This result implies that T-BiOCl (001) indeed has improved photocatalytic kinetics compared to the BiOCl (001).

The photocatalytic degradation of toxic pollutants or organic dyes, which is significant in environment purification, represents a generally utilized approach to evaluate the performance of photocatalysts. The photocatalytic activities of T-BiOCl (001) are evaluated under UV light illumination with

dx.doi.org/10.1021/am5052526 | ACS Appl. Mater. Interfaces 2014, 6, 18423−18428

MO as probe molecules in aqueous solution, and the corresponding activities for the BiOCl (001) nanosheets is likewise supplied for comparison. The photodegradation of MO is carried out via a direct semiconductor photoexcitation process under UV irradiation. The photodegradation of MO is negligible in the absence of photocatalyst under UV irradiation (Figure 5a). The photolytic fade in the presence T-BiOCl (001) and BiOCl (001) in the dark is only approximately 4.1% and 5.9% after 60 min (Figure 5b). As illustrated in Figure 4a, the photodegradation percentages of MO are 95% and 33% for T-BiOCl (001) and BiOCl (001) after ultraviolet illumination for 60 min. The N_2 sorption analysis results (Figure 5c) show that the BET specific surface areas for the as-sythesized BiOCl (001) and T-BiOCl (001) are ca. 1.4 $m^2 g^{-1}$ and ca. 1.6 $m^2 g^{-1}$, confirming that the higher adsorption capacity of T-BiOCl (001) could be attributed to the surface area factor. In order to describe the photocatalytic performance more accurately, the initial reaction rate of photocatalytic degradation is investigated. For the low concentration of the original solution, the catalytic activity are supposed to accord with a first-order reaction kinetics model and the result is illustrated in Figure S7 in the Supporting Information.[23] The degradation constant of T-BiOCl (001) ($k' = 3.0 \times 10^{-2}$ g min^{-1} m^{-2}) is much higher than BiOCl (001) ($k' = 4.5 \times 10^{-3}$ g min^{-1} m^{-2}) after normalized with surface areas (Figure 5d). The results above clearly demonstrate that the superior photocatalytic performance of T-BiOCl (001) should be associated with the unique topotactic homogeneous and teethlike structure rather than surface area.

In summary, a novel teethlike layered homogeneous structural BiOCl (001) nanosheets is sythesized by selective etching using TEA. Structural and compositional analyses show that the products are constructed via large number of ultrathin teethlike BiOCl nanosheets attached to the fringe planes of BiOCl (001) and (001) plane perfectly retained. With respect to BiOCl (001), T-BiOCl (001) exhibits a superior photocatalytic activity which can be ascribed to the combined interaction of the high UV/vis light harvest, high photogenerated charges separation efficiency, and the fast interfacial charge-transfer rate based on the unique homogeneous topotactic structure. Because layered 2D semiconductors are quite common in nature, an atomically homogeneous junction in one a single 2D semiconductor with different thickness can be conveniently fabricated by etching or exfoliating. The approach of homogeneous junction described here will open a new avenue for the development of efficient photocatalysts.

■ ASSOCIATED CONTENT

Ⓢ Supporting Information

Experimental details and additional supporting data such as the high magnification SEM images of T-BiOCl (001), XRD patterns, FTIR spectra, Raman spectrum, XPS spectra and ESR spectra of BiOCl (001) and T-BiOCl (001), atomic structure of the (001) facet and Kinetic analysis of the emission decay of the different samples. This material is available free of charge via the Internet at http://pubs.acs.org.

■ AUTHOR INFORMATION

Corresponding Author

*Tel./fax: +86 591 83779239. E-mail: liuping@fzu.edu.cn.

Notes

The authors declare no competing financial interest.

■ ACKNOWLEDGMENTS

The work is supported by National Natural Science Foundation of China (21173046, 21033003, 21273035 and 21473031), National Basic Research Program of China (973 Program: 2013CB632405).

■ REFERENCES

(1) Novoselov, K. S.; Jiang, D.; Schedin, F.; Booth, T. J.; Khotkevich, V. V.; Morozov, S. V.; Geim, A. K. Two-dimensional Atomic Crystals. *Proc. Natl. Acad. Sci. U. S. A.* **2005**, *102*, 10451−10453.

(2) Huang, X.; Qi, X.; Boey, F.; Zhang, H. Graphene-based Composites. *Chem. Soc. Rev.* **2012**, *41*, 666−686.

(3) Zhang, X.; Xie, Y. Recent Advances in Free-standing Two-dimensional Crystals with Atomic Thickness: Design, Assembly and Transfer Strategies. *Chem. Soc. Rev.* **2013**, *42*, 8187−8199.

(4) Ye, L.; Zan, L.; Tian, L.; Peng, T.; Zhang, J. The {001} Facets-dependent High Photoactivity of BiOCl Nanosheets. *Chem. Commun.* **2011**, *47*, 6951−6953.

(5) Jiang, J.; Zhao, K.; Xiao, X.; Zhang, L. Synthesis and Facet-dependent Photoreactivity of BiOCl Single-crystalline Nanosheets. *J. Am. Chem. Soc.* **2012**, *134*, 4473−4476.

(6) Weng, S.; Chen, B.; Xie, L.; Zheng, Z.; Liu, P. Facile in situ Synthesis of A Bi/BiOCl Nanocomposite with High Photocatalytic Activity. *J. Mater. Chem. A* **2013**, *1*, 3068−3075.

(7) Xiong, J. Y.; Cheng, G.; Li, G. F.; Qin, F.; Chen, R. Well-crystallized Square-like 2D BiOCl Nanoplates: Mannitol-assisted Hydrothermal Synthesis and Improved Visible-light-driven Photocatalytic Performance. *RSC Adv.* **2011**, *1*, 1542−1553.

(8) Tian, F.; Xiong, J. Y.; Zhao, H. P.; Liu, Y. L.; Xiao, S. Q.; Chen, R. Mannitol-assisted Solvothermal Synthesis of BiOCl Hierarchical Nanostructures and Their Mixed Organic Dye Adsorption Capacities. *CrystEngComm* **2014**, *16*, 4298−4305.

(9) Wang, D. H.; Gao, G. Q.; Zhang, Y. W.; Zhou, L. S.; Xu, A. W.; Chen, W. Nanosheet-constructed Porous BiOCl with Dominant {001} Facets for Superior Photosensitized Degradation. *Nanoscale* **2012**, *4*, 7780−7785.

(10) Zhang, X.; Wang, X. B.; Wang, L. W.; Wang, W. K.; Long, L. L.; Li, W. W.; Yu, H. Q. Synthesis of a Highly Efficient BiOCl Single-crystal Nanodisk Photocatalyst with Exposing {001} Facets. *ACS Appl. Mater. Interfaces* **2014**, *6*, 7766−7772.

(11) Hou, Y.; Laursen, A. B.; Zhang, J.; Zhang, G.; Zhu, Y.; Wang, X.; Dahl, S.; Chorkendorff, I. Layered Nanojunctions for Hydrogen-Evolution Catalysis. *Angew. Chem., Int. Ed.* **2013**, *52*, 3621−3625.

(12) Kim, H. G.; Borse, P. H.; Choi, W.; Lee, J. S. Photocatalytic Nanodiodes for Visible-light Photocatalysis. *Angew. Chem., Int. Ed.* **2005**, *44*, 4585−4589.

(13) Hong, S. J.; Lee, S.; Jang, J. S.; Lee, J. S. Heterojunction $BiVO_4$/WO_3 Electrodes for Enhanced Photoactivity of Water Oxidation. *Energy Environ. Sci.* **2011**, *4*, 1781−1787.

(14) Zong, X.; Yan, H.; Wu, G.; Ma, G.; Wen, F.; Wang, L.; Li, C. Enhancement of Photocatalytic H_2 Evolution on CdS by Loading MoS_2 as Cocatalyst under Visible Light Irradiation. *J. Am. Chem. Soc.* **2008**, *130*, 7176−7177.

(15) Zhang, J.; Xu, Q.; Feng, Z.; Li, M.; Li, C. Importance of The Relationship between Surface Phases and Photocatalytic Activity of TiO_2. *Angew. Chem., Int. Ed.* **2008**, *47*, 1766−1769.

(16) Yu, C.; Li, G.; Kumar, S.; Yang, K.; Jin, R. Phase Transformation Synthesis of Novel Ag_2O/Ag_2CO_3 Heterostructures with High Visible Light Efficiency in Photocatalytic Degradation of Pollutants. *Adv. Mater.* **2014**, *26*, 892−898.

(17) Yu, C.; Wei, L.; Chen, J.; Xie, Y.; Zhou, W.; Fan, Q. Enhancing the Photocatalytic Performance of Commercial TiO_2 Crystals by Coupling with Trace Narrow-Band-Gap Ag_2CO_3. *Ind. Eng. Chem. Res.* **2014**, *53*, 5759−5766.

(18) Wang, X.; Xu, Q.; Li, M.; Shen, S.; Wang, X.; Wang, Y.; Feng, Z.; Shi, J.; Han, H.; Li, C. Photocatalytic Overall Water Splitting Promoted by an α−β phase Junction on Ga_2O_3. *Angew. Chem., Int. Ed.* **2012**, *51*, 13089−13092.

(19) Zhang, J.; Zhang, M.; Sun, R. Q.; Wang, X. A Facile Band Alignment of Polymeric Carbon Nitride Semiconductors to Construct Isotype Heterojunctions. *Angew. Chem., Int. Ed.* **2012**, *51*, 10145−10149.
(20) Guan, M.; Xiao, C.; Zhang, J.; Fan, S.; An, R.; Cheng, Q.; Xie, J.; Zhou, M.; Ye, B.; Xie, Y. Vacancy Associates Promoting Solar-driven Photocatalytic Activity of Ultrathin Bismuth Oxychloride Nanosheets. *J. Am. Chem. Soc.* **2013**, *135*, 10411−10417.
(21) Hancock, R. D.; Cukrowski, I.; Baloyi, J.; Mashishi, J. The Affinity of Bismuth(III) for Nitrogen-donor Ligands. *J. Chem. Soc., Dalton Trans.* **1993**, 2895−2899.
(22) Zhu, J.; Wang, J.; Lv, F.; Xiao, S.; Nuckolls, C.; Li, H. Synthesis and Self-Assembly of Photonic Materials from Nanocrystalline Titania Sheets. *J. Am. Chem. Soc.* **2013**, *135*, 4719−4721.
(23) Wang, X. H.; Li, J. G.; Kamiyama, H.; Moriyoshi, Y.; Ishigaki, T. Wavelength-Sensitive Photocatalytic Degradation of Methyl Orange in Aqueous Suspension over Iron(III)-doped TiO2 Nanopowders under UV and Visible Light Irradiation. *J. Phys. Chem. B* **2006**, *110*, 6804−6809.